Parametric Imaging and Test–Retest Variability of ^{11}C-(+)-PHNO Binding to D_2/D_3 Dopamine Receptors in Humans on the High-Resolution Research Tomograph PET Scanner

Jean-Dominique Gallezot[1], Ming-Qiang Zheng[1], Keunpoong Lim[1], Shu-fei Lin[1], David Labaree[1], David Matuskey[1,2], Yiyun Huang[1], Yu-Shin Ding[1,3], Richard E. Carson[1], and Robert T. Malison[2]

[1]PET Center, Department of Diagnostic Radiology, Yale University School of Medicine, New Haven, Connecticut; [2]Department of Psychiatry, Yale University School of Medicine, New Haven, Connecticut; and [3]Department of Radiology and Psychiatry, New York University School of Medicine, New York, New York

^{11}C-(+)-4-propyl-9-hydroxynaphthoxazine (^{11}C-(+)-PHNO) is an agonist radioligand for imaging dopamine D_2 and D_3 receptors in the human brain with PET. In this study we evaluated the reproducibility of ^{11}C-(+)-PHNO binding parameters using a within-day design and assessed parametric imaging methods. **Methods:** Repeated studies were performed in 8 subjects, with simultaneous measurement of the arterial input function and plasma free fraction. Two ^{11}C-(+)-PHNO scans for the same subject were separated by 5.4 ± 0.7 h. After compartment models were evaluated, ^{11}C-(+)-PHNO volumes of distribution (V_T) and binding potentials relative to the concentration of tracer in plasma (BP_P), nondisplaceable tracer in tissue (BP_{ND}), and free tracer in tissue (BP_F) were quantified using the multilinear analysis MA1 method, with the cerebellum as the reference region. Parametric images of BP_{ND} were also computed using the simplified reference tissue model (SRTM) and SRTM2. **Results:** The test–retest variability of ^{11}C-(+)-PHNO BP_{ND} was 9% in D_2-rich regions (caudate and putamen). Among D_3-rich regions, variability was low in the pallidum (6%) but higher in substantia nigra (19%), thalamus (14%), and hypothalamus (21%). No significant mass carry-over effect was observed in D_3-rich regions, although a trend in BP_{ND} was present in the substantia nigra (−14% ± 15%). Because of the relatively fast kinetics, low-noise BP_{ND} parametric images were obtained with both SRTM and SRTM2 without spatial smoothing. **Conclusion:** ^{11}C-(+)-PHNO can be used to compute low-noise parametric images in both D_2- and D_3-rich regions in humans.

Key Words: dopamine D2 receptor; dopamine D3 receptor; agonist; positron emission tomography; test–retest study

J Nucl Med 2014; 55:960–966
DOI: 10.2967/jnumed.113.132928

The tracer ^{11}C-(+)-4-propyl-9-hydroxynaphthoxazine (^{11}C-(+)-PHNO) is used to study dopamine D_2 and D_3 receptors (D2R and D3R) in vivo with PET (*1*). As an agonist tracer (*2*), ^{11}C-(+)-PHNO is useful to study the high-affinity states of D2R/D3R and to amplify the signal in studies of dopamine release (*3*). Other available D2R/D3R agonist radioligands include (−)-*N*-^{11}C-propyl-norapomorphine (^{11}C-NPA) and [*O*-methyl-^{11}C]2-methoxy-*N*-propyl-norapomorphine (^{11}C-MNPA). In contrast to existing radioligands, however, ^{11}C-(+)-PHNO is D3R-preferring, with a 30- to 50-fold higher affinity for D3R than for D2R both in vitro (*4*) and in vivo (*5*). Therefore, ^{11}C-(+)-PHNO–specific binding derives from contributions of both D2R and D3R, in proportions that vary across regions based on their respective densities. The D3R fraction of specific binding ranges from 0% in the putamen to 100% in the substantia nigra (SN) and hypothalamus in humans (*6*). Though ^{11}C-(+)-PHNO is not a perfectly selective D3R radioligand, it is, to date, the most specific radioligand available to assess D3R in vivo in humans (*7*).

Kinetic modeling of ^{11}C-(+)-PHNO has been performed previously in humans (*8*). For studies with arterial blood sampling, a constrained form of the 2-tissue-compartment (2TC) model was selected as the method of choice to estimate BP_{ND} binding potentials, and for studies without arterial blood sampling, the simplified reference tissue model (SRTM) provided highly correlated outcomes (albeit with a 10% underestimation of BP_{ND}) (*9*). One goal of the present study was to evaluate the test–retest (T-R) variability (TRV) of ^{11}C-(+)-PHNO parameter estimates using a within-day design and the high-resolution PET scanner, High-Resolution Research Tomograph (HRRT; Siemens/CTI). The latter is especially relevant in light of the regional D3R specificity of small structures, such as the SN. The second goal of this study was to evaluate strategies for computing parametric images of ^{11}C-(+)-PHNO binding potentials to minimize image noise while using the lowest amount of spatial smoothing possible, for purposes of elucidating receptor topology at high resolution. In addition, potential mass carry-over effect on binding parameters, as seen in previous preclinical studies (*10*), was also investigated in this within-day, repeated-scan paradigm, particularly in high-affinity D3R-rich regions.

MATERIALS AND METHODS

Subjects

Eight subjects (7 men, 1 woman) were included in the study: 5 were healthy controls (HCs) and 3 were cocaine-dependent (CD) according to the *Diagnostic and Statistical Manual of Mental Disorders* (DSM-IV) (*11*) criteria. We purposefully included a patient group in the T-R assessment (see the "Discussion" section). The average age and weight were 35 ± 9 y and 80 ± 16 kg, respectively. The absence of recent substance use was confirmed by urine toxicology on both the day of screening and the day of PET scanning, before tracer injection.

The study was performed under protocols approved by the Yale School of Medicine Human Investigation Committee, the Human

Received Sep. 27, 2013; revision accepted Jan. 21, 2014.
For correspondence or reprints contact: Jean-Dominique Gallezot, PET Center, Yale University, 801 Howard Ave., P.O. Box 208048, New Haven, CT 06520-8048.
E-mail: jean-dominique.gallezot@yale.edu
Published online Apr. 14, 2014.

Subjects Subcommittee of the Veterans Affairs Connecticut Healthcare System, the Yale-New Haven Hospital Radiation Safety Committee, and the Yale University Radiation Safety Committee. Subjects were recruited by public advertisement. Written informed consent was obtained from all participants after full explanation of study procedures.

Radiochemistry

^{11}C-(+)-PHNO was prepared by *N*-acylation of the norpropyl precursor with ^{11}C-propionyl chloride, followed by reduction of the resulting amide with lithium aluminum hydride and purification by reversed-phase high-performance liquid chromatography, in a modified literature procedure (*1*). The supplemental information provides details (supplemental materials are available at http://jnm.snmjournals.org). The radiochemical and chemical purity were greater than 98% and greater than 99%, respectively, and the specific activity at the end of synthesis was 83 ± 35 MBq/nmol.

PET Imaging

Each subject underwent 2 PET scans on the same day, separated by 5.4 ± 0.7 h (minimum, 4.5 h), on the HRRT. ^{11}C-(+)-PHNO (328 ± 103 MBq) was injected by a computer-controlled infusion pump (Harvard PHD 22/2000; Harvard Apparatus). The tracer specific activity at the time of injection was 45 ± 18 MBq/nmol. The injected mass was 25 ± 5 ng/kg (maximum, 31 ng/kg). The injected dose, injected mass, and specific activity did not differ significantly between the test and retest scans (paired *t* test, $P = 0.13$, 0.97, and 0.60, respectively) (Table 1). The metabolite-corrected arterial input function and the plasma free fraction (f_P) of ^{11}C-(+)-PHNO were measured. The supplemental information provides details.

Quantification of PET Data

Gray matter regions of interest (ROIs) were taken from the anatomic automatic labeling template. Six ROIs were selected: cerebellum, caudate, putamen, pallidum, amygdala, and thalamus. Extra ROIs corresponding to the hypothalamus and ventral striatum were also drawn on the template MR image, and an SN template ROI was also created using PET images (supplemental information). The template ROIs were applied to the PET data using nonlinear transforms (supplemental information).

On the basis of a previous report (*8*), the 2TC model and multilinear analysis (MA1) method (*12*) were evaluated to quantify the volume of distribution (V_T) (*9*) using arterial blood sampling. To compare the quality of fit between the 1TC and 2TC models, the residual sum of square was compared with the F test, using a cutoff *P* value of 0.05 corrected for the number of comparisons (i.e., the number of scans, 16). For MA1, the starting time of the fit, *t**, was set to 30 min. On the basis of the V_T values, 3 versions of the binding potential (BP_F, BP_P, and BP_{ND}) (*9*) were calculated, with the cerebellum used as the reference region. In addition, the SRTM (*13*) was used to estimate ^{11}C-(+)-PHNO BP_{ND} without arterial blood sampling.

For parametric imaging, both the SRTM (*13*) and the SRTM2 (*14*) methods were tested. Both SRTM and SRTM2 were implemented using a basis-function approach restricting the parameter k_2 (the clearance rate constant of each voxel) to the range of 0.01–1.0 min^{-1}. No spatial smoothing was applied. In SRTM2, the clearance rate constant of the reference region, k_2', was estimated from SRTM parametric images as the median k_2' estimate from brain voxels where BP_{ND} was greater than 0.5. ROIs, as described above, were applied to the parametric images, and the mean values for BP_{ND} were compared with those obtained by fits of regional time–activity curves.

TRV Estimation

TRV was estimated for each parameter of interest *p* by computing first Δp as defined below:

$$\Delta p = 2\frac{p^{retest} - p^{test}}{p^{retest} + p^{test}} \qquad \text{Eq. 1}$$

and then by computing the means of Δp across subjects (noted as $m(\Delta p)$) and the SD of Δp across subjects (noted as $\sigma(\Delta p)$), with $m(\Delta p)$ indicating whether there is a trend between the 2 scans for the parameter of interest *p* and $\sigma(\Delta p)$ as an index of the variability for the estimates of the parameter of interest *p*. An alternate index of the variability for the estimates of the parameter of interest *p* was also computed as the mean across subjects of the absolute value of Δp and noted as $m(|\Delta p|)$. For comparison with a previous study (*15*), $\sigma(\delta p)$ was computed, where $\delta p = (p^{retest} - p^{test})/p^{test}$. Finally, the intraclass correlation coefficient (ICC) was also computed as in the study of Shrout and Fleiss (*16*). Because this study includes HCs and CD subjects, the between-subject variance is larger than what would be present in a single-group study, causing the ICC values to be increased (see the "Discussion" section).

For parametric images, TRV was computed in 2 ways: first, to estimate variability in ROI-based analyses, TRV was computed using the regional averages of the parametric images. Second, to assess variability for statistical analyses of parametric images, test and retest parametric images were resliced to the ROI template space, images of $\sigma(\Delta p)$ and $m(|\Delta p|)$ were generated in template space, and finally the median of $\sigma(\Delta p)$ and $m(|\Delta p|)$ within each ROI was computed.

RESULTS

Kinetic Analysis with Arterial Input Function

In the pallidum, hypothalamus, ventral striatum, and SN, the 2TC model provided better fits than the 1-tissue-compartment (1TC) model for all subjects and scans ($F_{2,29}$, $P < 0.003$). In other regions, 2TC provided better fits for most scans. However, 2TC did not provide reliable V_T estimates in most regions, with at least 25% of the V_T relative SEs (%SE) being higher than 50% in the cerebellum, putamen, ventral striatum, hypothalamus, and SN and ICC values for V_T estimates being lower than 0.03.

TABLE 1
Synthesis and Injection Parameters

Parameter	Test scan	Retest scan	Variation*
Specific activity at end of synthesis (MBq/nmol)	76 ± 30	90 ± 38	27% ± 57%
Specific activity at time of injection (MBq/nmol)	42 ± 17	47 ± 17	25% ± 58%
Injected dose (MBq)	315 ± 111	342 ± 93	13% ± 19%
Injected mass (ng/kg)	25 ± 5	25 ± 6	6% ± 39%

*Computed as retest value/test value – 1.

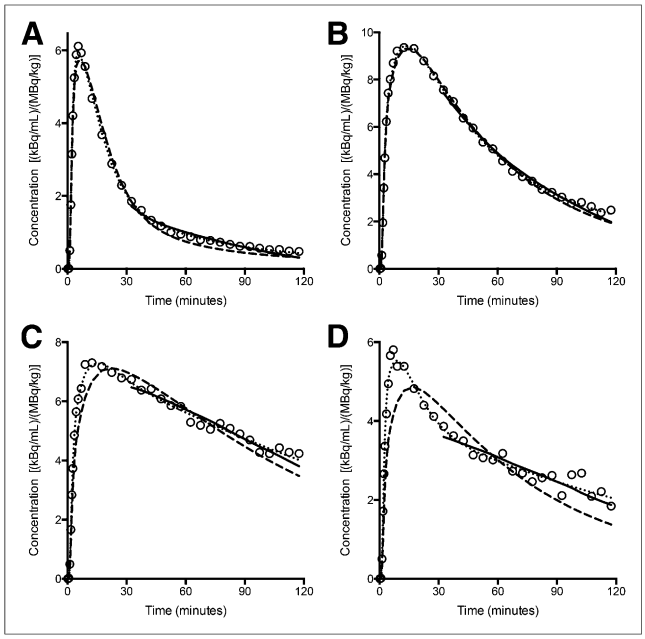

FIGURE 1. Sample fits obtained with MA1 (solid line) and with 1TC (dashed line) and 2TC (dotted line) models in 1 typical subject's test scan. Data are derived from standardized uptake values in cerebellum (A), putamen (B), pallidum (C), and SN (D).

Because of the variability in 2TC V_T estimates, MA1 was also evaluated. Typical fits obtained with MA1, 1TC, and 2TC models are shown in Figure 1. For the subset of regions and scans for which the 2TC V_T %SE was lower than 5%, the V_T values estimated with MA1 ($t^* = 30$ min) and 2TC were nearly identical ($r^2 = 0.996$, $y = 0.97x + 0.17$, where x represents the 2TC estimates and y represents the MA1 estimates). With MA1, the %SE of V_T was less than 5% for all scans in the amygdala, caudate, putamen, pallidum, and thalamus. In the SN, ventral striatum, and hypothalamus, the highest %SEs were 12%, 7%, and 12%, respectively.

The MA1 parameter estimates from the test scan for HCs ($n = 5$) and the T-R statistics for all subjects ($n = 8$) are listed in Table 2. There were no significant differences between test and retest V_T in any ROI (paired t test; P value from 0.37 to 0.92), and the mean relative change of V_T, $m(\Delta V_T)$, ranged between −9% and +2%. The variability of V_T ($\sigma(\Delta V_T)$) ranged from 13% in the putamen to 25% in the SN. The means of the absolute values of ΔV_T, $m(|\Delta V_T|)$, were lower than $\sigma(\Delta V_T)$ and ranged from 9% to 21% (see the "Discussion" section). The ICC values for V_T estimates ranged from 0.28 in the cerebellum to 0.88 in the pallidum. The f_P was 0.44 ± 0.03 ($n = 5$) for the test scans, with no T-R change ($\Delta f_P = 0\% \pm 7\%$, $n = 8$; $P = 0.88$, paired t test; $m(|\Delta f_P|) = 5\%$). Normalizing V_T by f_P did not change TRV (supplemental information). $\sigma(\Delta BP_{ND})$ ranged from 10% to 29%, and $m(|\Delta BP_{ND}|)$ ranged from 6% to 25%. The variability of BP_P and BP_F was approximately 22% and approximately 13% higher, respectively, than that of BP_{ND} (based on $\sigma(\Delta p)$) (supplemental information). The ICC values for MA1 BP_{ND} estimates ranged from 0.29 in the amygdala to 0.92 in the SN and caudate.

Kinetic Analysis with Reference Region

SRTM BP_{ND} in the caudate, putamen, pallidum, and SN was well correlated with BP_{ND} estimated with MA1. The parameters of the regression line between MA1 and SRTM BP_{ND} values were slope = 0.966 ± 0.012, intercept = 0.080 ± 0.032, and $r^2 = 0.984$. The thalamus was not included in this comparison because SRTM BP_{ND} estimates in the thalamus had poor identifiability (maximum %SE > 100%; $\Delta BP_{ND} = 1\% \pm 105\%$). TRV indices for SRTM BP_{ND} are listed in Table 3. The variability of SRTM BP_{ND} estimates was similar to that of MA1 BP_{ND} estimates in the basal ganglia and SN (neither ΔBP_{ND} nor $|\Delta BP_{ND}|$ was significantly different between these 2 methods in these ROIs: paired Student t test $P > 0.11$). The ICC values for SRTM BP_{ND} estimates ranged from 0.06 in the hypothalamus to 0.92 in the caudate.

Parametric Imaging

Typical SRTM and SRTM2 parametric images are shown in Figure 2. Visually, SRTM and SRTM2 BP_{ND} images are similar, with slightly lower noise in SRTM2 images (noise reduction is more visible in low-binding regions or near high-BP_{ND} areas) but also slightly lower BP_{ND} values in D_3-rich regions. There was a visually bigger reduction of noise with SRTM2 for delivery (R_1) images. The variability of the parametric images was quantified by

TABLE 2
V_T and BP_{ND} Estimates for MA1 Fits of Regional Time–Activity Curves

Region	V_T			BP_{ND}		
	Average*	ΔV_T†	ICC‡	Average*	ΔBP_{ND}§	ICC‡
Cerebellum	4.7 ± 0.7 (14%)	2% ± 18% (12%)	0.28 (−0.44; 0.79)			
Caudate	13.2 ± 1.8 (14%)	0% ± 15% (11%)	0.81 (0.35; 0.96)	1.8 ± 0.2 (9%)	−2% ± 10% (9%)	0.92 (0.69; 0.98)
Putamen	15.8 ± 1.9 (12%)	−1% ± 13% (9%)	0.72 (0.16; 0.94)	2.4 ± 0.2 (8%)	−4% ± 11% (9%)	0.57 (−0.11; 0.89)
Pallidum	20.1 ± 3.2 (16%)	−2% ± 14% (9%)	0.88 (0.54; 0.97)	3.3 ± 0.6 (17%)	−6% ± 11% (6%)	0.87 (0.51; 0.97)
Ventral striatum	22.2 ± 4.9 (22%)	0% ± 21% (15%)	0.64 (0.01; 0.92)	3.7 ± 0.6 (15%)	−2% ± 12% (10%)	0.82 (0.38; 0.96)
Amygdala	5.9 ± 0.8 (14%)	−1% ± 15% (10%)	0.51 (−0.19; 0.88)	0.26 ± 0.07 (26%)	−13% ± 29% (25%)	0.29 (−0.42; 0.80)
SN	13.4 ± 2.6 (19%)	−9% ± 25% (21%)	0.85 (0.45; 0.97)	1.8 ± 0.4 (19%)	−16% ± 17% (19%)	0.92 (0.68; 0.98)
Thalamus	6.4 ± 1.2 (18%)	2% ± 17% (13%)	0.55 (−0.13; 0.89)	0.36 ± 0.10 (28%)	2% ± 19% (14%)	0.73 (0.17; 0.94)
Hypothalamus	12.4 ± 2.7 (22%)	−3% ± 14% (11%)	0.80 (0.32; 0.95)	1.7 ± 0.8 (48%)	−7% ± 27% (21%)	0.55 (−0.14; 0.89)

*$n = 5$ HCs; data are presented as mean ± SD (relative SD) across subjects.
†$n = 8$ subjects; data are presented as $m(\Delta V_T) \pm \sigma(\Delta V_T)$ ($m(|\Delta V_T|)$).
‡$n = 8$ subjects; ICC is presented as estimate, with lower and upper bounds of 95% confidence interval in parentheses.
§$n = 8$ subjects; data are presented as $m(\Delta BP_{ND}) \pm \sigma(\Delta BP_{ND})$ ($m(|\Delta BP_{ND}|)$).

TABLE 3
BP_{ND} Estimates for SRTM Fits of Regional Time–Activity Curves

Region	Average*	ΔBP_{ND}†	ICC‡
Caudate	1.8 ± 0.1 (8%)	−3% ± 9% (8%)	0.92 (0.70; 0.98)
Putamen	2.4 ± 0.2 (8%)	−4% ± 10% (9%)	0.59 (−0.07; 0.90)
Pallidum	3.3 ± 0.6 (18%)	−4% ± 12% (8%)	0.81 (0.36; 0.96)
Ventral striatum	3.6 ± 0.4 (12%)	−1% ± 13% (12%)	0.74 (0.20; 0.94)
Amygdala	0.29 ± 0.16 (54%)	−22% ± 41% (36%)	0.15 (−0.54; 0.74)
SN	2.0 ± 0.3 (13%)	−19% ± 18% (20%)	0.86 (0.50; 0.97)
Thalamus	0.38 ± 0.11 (29%)§	1% ± 105% (71%)	0.33 (−0.39; 0.81)
Hypothalamus	2.6 ± 2.5 (95%)	−14% ± 54% (38%)	0.06 (−0.60; 0.69)

*n = 5 HCs; data are presented as mean ± SD (relative SD) across subjects.
†n = 8 subjects; data are presented as $m(\Delta BP_{ND}) \pm \sigma(\Delta BP_{ND})$ ($m(|\Delta BP_{ND}|)$).
‡n = 8 subjects; ICC is presented as estimate, with lower and upper bounds of 95% confidence interval in parentheses.
§Excluding 1 outlier.

computing parametric images of $\sigma(\Delta R_1)$ and $\sigma(\Delta BP_{ND})$ in template space. The median value in each ROI is reported in Supplemental Table 3. The median of $\sigma(\Delta R_1)$ ranged from 20% to 37% with SRTM and from 14% to 23% with SRTM2, and the improvement with SRTM2 ranged from 2 percentage points (in the SN) to 14 percentage points (in the amygdala). The median of $\sigma(\Delta BP_{ND})$ ranged from 34% (in the caudate) to 155% (in the amygdala) with SRTM and from 22% (in the caudate) to 86% (in the amygdala) with SRTM2, and the improvement with SRTM2 ranged from −1 percentage point in the hypothalamus to 69 percentage points in the amygdala.

ROI values from the parametric images (Table 4) were well correlated with BP_{ND} estimated from fits of regional time–activity curves. The regression parameters between MA1 and parametric BP_{ND} were slope = 0.888 ± 0.018, intercept = 0.219 ± 0.047, and r^2 = 0.952 for SRTM and slope = 0.861 ± 0.019, intercept = 0.133 ± 0.048, and r^2 = 0.941 for SRTM2. At the regional average level, SRTM2 and SRTM BP_{ND} were highly correlated (slope = 0.971 ± 0.009, intercept = –0.081 ± 0.021, and r^2 = 0.990), though SRTM2 values were slightly lower than SRTM values, with relative differences ranging from 0% ± 2% in the putamen to −19% ± 7% in the hypothalamus, with −12% ± 8% in the SN (significant in all regions except the putamen).

TRV indices and ICC values of regional averages from SRTM and SRTM2 parametric images are listed in Table 4. The variability of SRTM and SRTM2 values was similar to that of MA1 BP_{ND} estimates in all ROIs.

Carry-over Mass Effect

There were no significant differences between test and retest BP_{ND} in any ROI outside the SN (paired t test; P = 0.14–0.95). In the SN, there was a trend level or significant reduction in BP_{ND} in the retest scans depending on the method. The P values were 0.06 with MA1 and less than 0.05 with SRTM and parametric SRTM and SRTM2 (paired t test; n = 8). The average reduction of the SN BP_{ND} across all methods was −14% ± 15%.

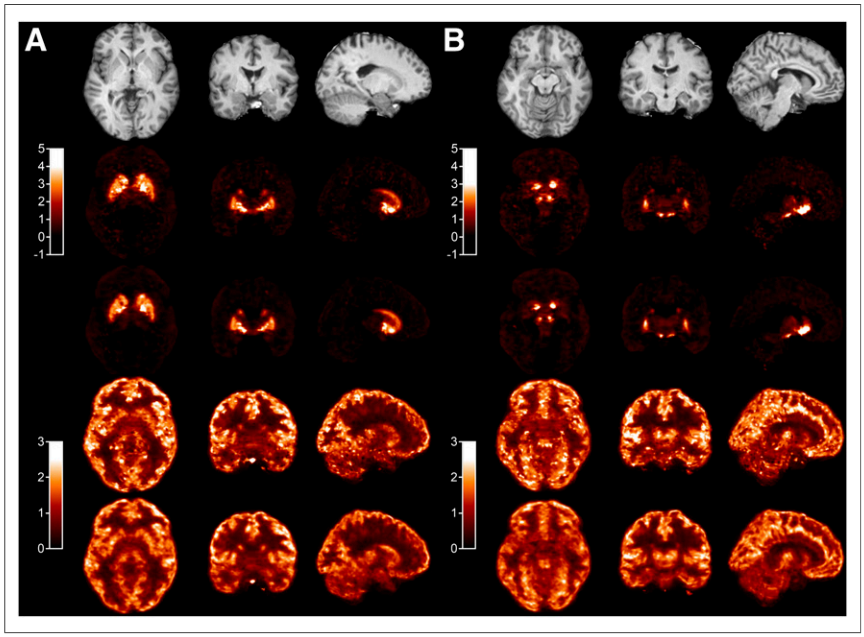

FIGURE 2. Typical parametric images at level of pallidum (A) and SN (B). Row 1 is coregistered MR image; row 2, SRTM BP_{ND}; row 3, SRTM2 BP_{ND}; row 4, SRTM R_1 (relative delivery); and row 5, SRTM2 R_1.

DISCUSSION

The current study extends evaluations of optimal image and data analyses for ^{11}C-(+)-PHNO–bolus-injection PET studies in humans using multiple modeling methods, parametric imaging, and T-R studies. A detailed comparison of kinetic modeling methods for quantifying ^{11}C-(+)-PHNO binding in humans has been published previously (*8*). In that study, the 2TC model was the method of choice to estimate ^{11}C-(+)-PHNO V_T. However, in the current study, high %SE was observed in some scans and ROIs. The differences between these 2 studies may also be due to different noise properties of the 2 datasets (both were acquired on the same type of scanner but with different reconstruction algorithms), differences in the delineation of the regions of interest, or differences in the fitting routines and settings.

TABLE 4
Regional BP_{ND} Values from Parametric Maps

Region	SRTM			SRTM2		
	Average*	ΔBP_{ND}†	ICC‡	Average*	ΔBP_{ND}†	ICC‡
Caudate	2.0 ± 0.1 (7%)	−3% ± 9% (8%)	0.92 (0.68; 0.98)	1.9 ± 0.2 (10%)	−3% ± 10% (9%)	0.91 (0.65; 0.98)
Putamen	2.6 ± 0.2 (8%)	−4% ± 11% (9%)	0.63 (−0.01;0.91)	2.5 ± 0.2 (9%)	−4% ± 11% (9%)	0.59 (−0.07; 0.90)
Pallidum	3.3 ± 0.5 (15%)	−4% ± 11% (7%)	0.76 (0.23; 0.95)	3.2 ± 0.6 (18%)	−5% ± 12% (8%)	0.76 (0.24; 0.95)
Ventral striatum	3.8 ± 0.4 (10%)	−1% ± 11% (9%)	0.80 (0.33; 0.96)	3.5 ± 0.5 (13%)	−2% ± 12% (8%)	0.80 (0.34; 0.96)
Amygdala	0.32 ± 0.07 (23%)	−11% ± 24% (21%)	0.32 (−0.40; 0.81)	0.27 ± 0.08 (28%)	−12% ± 28% (24%)	0.30 (−0.42; 0.80)
SN	1.8 ± 0.3 (16%)	−9% ± 12% (11%)	0.94 (0.77; 0.99)	1.6 ± 0.4 (24%)	−11% ± 14% (12%)	0.95 (0.79; 0.99)
Thalamus	0.40 ± 0.12 (29%)	−1% ± 21% (15%)	0.71 (0.14; 0.93)	0.36 ± 0.09 (25%)	−1% ± 20% (15%)	0.50 (−0.20; 0.87)
Hypothalamus	1.6 ± 0.6 (36%)	−8% ± 22% (17%)	0.54 (−0.15; 0.88)	1.3 ± 0.6 (46%)	−9% ± 21% (16%)	0.61 (−0.05; 0.91)

*n = 5 HCs; data are presented as mean ± SD (relative SD) across subjects.
†n = 8 subjects; data are presented as $m(\Delta BP_{ND})$ ± $\sigma(\Delta BP_{ND})$ ($m(|\Delta BP_{ND}|)$).
‡n = 8 subjects; ICC is presented as estimate, with lower and upper bounds of 95% confidence interval in parentheses.

A method providing a compromise between the quality of fit of 2TC and the stability of V_T estimates was needed. The Logan graphical analysis was tested in the previous study and was found to provide V_T estimates highly correlated to, and not statistically different from, those obtained using unconstrained 2TC fits (*8*). However, the Logan graphical analysis is sensitive to noise, especially for small regions or single-voxel time–activity curves. The multilinear analysis MA1, which was designed to reduce this bias (*12*), was tested and proved to be the preferred method, as it provided more stable parameter estimates than 2TC.

In theory, SRTM is not a valid method for ^{11}C-(+)-PHNO because the regional time–activity curves are not well fitted with the 1TC model when the arterial input function is used. However, SRTM provided BP_{ND} estimates in good agreement with the MA1 estimates, which is partially in agreement with the earlier results (*8*): in that report, SRTM BP_{ND} estimates were in good agreement with BP_{ND} estimates with unconstrained 2TC fits (method B in the study by Ginovart et al. (*8*)), but they were lower than BP_{ND} estimates from constrained 2TC fits (method D in the study by Ginovart et al. (*8*)), the latter being the method of choice in that study. However, in the current study the good correlation between MA1 and SRTM BP_{ND} estimates was verified in a larger selection of ROIs, adding the SN, amygdala, and hypothalamus. SRTM2 also provided BP_{ND} estimates in good agreement with MA1 estimates.

In this study, 2 TRV indices were computed: $m(|\Delta p|)$ and $\sigma(\Delta p)$. The main advantage of computing the mean and SD of Δp ($m(\Delta p)$ and $\sigma(\Delta p)$) is that it can be used to assess whether there is a systematic trend or significant change in binding parameters between the test and retest scans. Computing only $m(|\Delta p|)$ does not permit the assessment of that trend. However, $m(|\Delta p|)$ and $\sigma(\Delta p)$ tend to provide numerically different indices for the variability of the parameter p, with $\sigma(\Delta p)$ being typically higher than $m(|\Delta p|)$. Indeed, for a gaussian variable p, with no trend between the test and retest scans (i.e., $m(\Delta p) = 0$), $m(|\Delta p|)$ is close to the relative SD of p, whereas $\sigma(\Delta p)$ is higher than the relative SD of p by a factor $\sqrt{2}$, because it represents the combined errors in the test and retest scans. On the other hand, $\sigma(\Delta p)$ will be close to the SD of Δp obtained in studies comparing baseline with postintervention scans, when the effect of the intervention is small. Thus, $\sigma(\Delta p)$ is useful to evaluate the possibility to detect small differences or effects. However, $m(|\Delta p|)$ is frequently used in the literature and, thus, is useful to be computed in addition to $\sigma(\Delta p)$ when tracers or methods are being compared.

Because of the high affinity of ^{11}C-(+)-PHNO for D3R and prior suggestions that PET studies performed using 0.03 μg/kg of ^{11}C-(+)-PHNO may not actually occur under true tracer conditions (*5,17*), it was postulated that binding potential estimates would be lower in D_3-rich regions during the same-day retest scanning. This was seen in a previous preclinical study (*10*), where the injected mass of ^{11}C-(+)-PHNO was approximately 0.04 μg/kg and the delay between injections was approximately 3 h and $m(\delta BP_{ND})$ ranged from −22% to −42% in D_3-rich regions. The current study was not designed to maximize chances of observing a carry-over mass effect but rather to evaluate whether such an effect could be detected despite the deliberate use of a longer (5-h) interval between ^{11}C-(+)-PHNO injections. As postulated, a significant reduction in BP_{ND} was detected in the SN in the retest scans, though this reduction was not significant with all methods and would not survive correction for multiple comparisons. The average $m(\Delta BP_{ND})$ was −14% across all methods. Three mechanisms for this carry-over effect are possible. First, sufficient unlabeled (+)-PHNO from the first injection might remain and compete for tracer binding during the second injection. Second, receptor changes in response to nontracer doses of the agonist during scan 1 are also possible (albeit unlikely here). Finally, we cannot rule out potential differences resulting from circadian variations, because by design all initial injections were around 10 AM and all second injections around 3–4 PM. The first hypothesis is compatible with estimates of the remaining concentration of (+)-PHNO during the second scan and previous estimates of the effective dose of (+)-PHNO inhibiting 50% of ^{11}C-(+)-PHNO–specific binding ((+)-PHNO ED_{50}). Indeed, during the first scan, the observed BP_{ND} would be given by the following equation:

$$BP_{ND}^{T} = BP_{ND}^{0} \times \left(1 - \frac{C}{C + IC_{50}}\right), \qquad \text{Eq. 2}$$

where BP_{ND}^{0} is the true binding potential at tracer dose, C is the concentration of tracer in tissue, and IC_{50} is the concentration of tracer to induce 50% reduction in binding. During the retest scan,

assuming that the injected dose is similar, the observed BP_{ND} would be:

$$BP^{R}_{ND} = BP^{0}_{ND} \times \left(1 - \frac{C \times (1+f)}{C \times (1+f) + IC_{50}}\right), \quad \text{Eq. 3}$$

where f is the fraction of tracer remaining from the first injection. Between the end of the first scan and the beginning of the second, the concentration of free (+)-PHNO in the SN may have decreased by 64%, based on extrapolation of the cerebellum curve, to 48%, based on extrapolation of the SN curve. To observe a mean ΔBP_{ND} value of 14% in such conditions, the concentration C in the above equations would need to be approximately 50% of the tracer IC_{50}. The average dose of ^{11}C-(+)-PHNO used in this study was 25 ng/kg, which is indeed close to 50% of the ^{11}C-(+)-PHNO $ED50$ estimated in a previous study (40 ng/kg) (*17*). Although there was no significant difference in the hypothalamus, another region in which approximately 100% of ^{11}C-(+)-PHNO BPND is due to D3R binding, there was, nonetheless, a similar trend ($m(\Delta BP_{ND})$ of −10% in average across all methods, which was not significant because of the higher variability of ^{11}C-(+)-PHNO BPND in this region.

When the various methods of computing BP_{ND} are compared, the variability of MA1 and SRTM estimates was comparable for ROI time–activity curve analyses, except in the thalamus, for which SRTM results were quite unreliable. When regional averages from parametric images were used, the variability of SRTM and SRTM2 BP_{ND} values was slightly lower than that of MA1 estimates. This effect was attributed to the choice of basis functions, which acted like a filter or a prior (see discussion below about parametric images). The ICC criterion leads to a similar conclusion: ICC values were slightly lower for SRTM BP_{ND} estimates than for MA1 BP_{ND} estimates, whereas ICC values for BP_{ND} values from parametric images (SRTM or SRTM2) were closer to the ICC values for MA1 BP_{ND} estimates.

The TRV of ^{11}C-(+)-PHNO BP_{ND} estimated with SRTM in this study was slightly better (lower) than in a previous study (*15*) for the caudate and putamen ($\sigma(\delta BP_{ND})$ was 9%–10%, vs. 12% in the previous study) and much lower for the pallidum ($\sigma(\delta BP_{ND})$ was 11% vs. 28% in the previous study). Conversely, the TRV of BP_{ND} estimated with SRTM in this study was slightly higher ($\sigma(\Delta BP_{ND})$ was 2% ± 4% higher on average for the caudate, putamen, pallidum, ventral striatum, and SN) than the variability of BP_{ND} estimated by equilibrium analysis using a bolus–infusion protocol (*18*).

In comparison to other tracers, the TRV of ^{11}C-(+)-PHNO V_T estimates was higher than that of ^{11}C-raclopride: $m(|\Delta V_T|)$ was 12% and 10% in the cerebellum and caudate/putamen for ^{11}C-(+)-PHNO versus 9% for ^{11}C-raclopride (*19*). Similarly, the TRV of ^{11}C-(+)-PHNO BP_{ND} was higher than that of ^{11}C-raclopride: $m(|\Delta BP_{ND}|)$ of 9% for ^{11}C-(+)-PHNO in the caudate/putamen versus only 4%–6% for ^{11}C-raclopride (*20*).

Compared with other D2R/D3R agonist radioligands, the TRV of ^{11}C-(+)-PHNO was also greater than that for ^{11}C-NPA, where $m(|\Delta V_T|)$ was 6%–9% and $m(|\Delta BP_{ND}|)$ was 4%–10%, depending on the region (*21*). Compared with ^{11}C-MNPA (*22*), ^{11}C-(+)-PHNO $m(|\Delta BP_{ND}|)$ was higher in the putamen (9% vs. 5%) and lower in the caudate (8% vs. 12%).

Parametric images were computed using SRTM and SRTM2 with a basis-function approach. Because of the relatively rapid kinetics of ^{11}C-(+)-PHNO, it was possible to obtain low-noise parametric images with both methods without spatial smoothing by restricting the range of the basis functions (restricting k_2 to be > 0.01 min^{-1}). Indeed, the basis functions used in the SRTM model are of the form $C_R(t) \otimes e^{-k_2 t}$, where $C_R(t)$ is the reference region time–activity curve. We chose to limit the k_2 values based on results of ROI time–activity curve analyses with SRTM2. Because of this restriction, SRTM parametric BP_{ND} images had relatively low noise, and the simplified model, SRTM2, mostly improved flow images (R_1) and BP_{ND} images outside the main ROIs.

In this T-R study, we intentionally included subjects who were not HCs. Including such subjects helped to ensure that the selected methods are applicable without major increases in TRV in subjects who may have atypical binding, because either higher or lower BP_{ND} in some regions can have an impact on the variability of the measures. On average, across all ROIs, the ratio of $m(|\Delta BP_{ND}|)$ in CD subjects and in HCs was 1.02, indicating that there was no global difference in variability between the 2 groups. The inclusion of noncontrol subjects can, however, have a bigger impact on ICC than TRV, because the ICC value is sensitive, by design, to the variability across subjects, which may be increased by including noncontrol subjects. This sensitivity of ICC to the study population does not prevent its use as a criterion to compare quantification methods but can be an issue when comparing results between studies on different populations (by diagnosis, age, or other demographic criteria influencing binding).

CONCLUSION

The TRV of ^{11}C-(+)-PHNO binding potential was 9% in the caudate and putamen, which is good, though higher than that of the leading antagonist, ^{11}C-raclopride, and other available agonists, including ^{11}C-NPA and ^{11}C-MNPA. Parametric images of ^{11}C-(+)-PHNO can be computed with low noise using both SRTM and SRTM2.

DISCLOSURE

The costs of publication of this article were defrayed in part by the payment of page charges. Therefore, and solely to indicate this fact, this article is hereby marked “advertisement” in accordance with 18 USC section 1734. This work was supported by a NARSAD Young Investigator Award grant (M132018), the National Institute on Drug Abuse (NIDA) (K24 DA017899; 1R03DA027456-01), the National Institute of Mental Health (NIMH; T32 MH019961), Yale PET Center and YCCI Pilot Projects Utilizing Core Technologies, and the Department of Mental Health and Addiction Services (DMHAS) of the State of Connecticut. This publication was also made possible by CTSA grant UL1 RR024139 from the National Center for Research Resources (NCRR) and the National Center for Advancing Translational Science (NCATS), components of the National Institutes of Health (NIH). Its contents are solely the responsibility of the authors and do not necessarily represent the official view of NIH. No other potential conflict of interest relevant to this article was reported.

ACKNOWLEDGMENT

We thank the staff of the Clinical Neuroscience Research Unit (CNRU) at Connecticut Mental Health Center (CMHC).

REFERENCES

1. Wilson AA, McCormick P, Kapur S, et al. Radiosynthesis and evaluation of [^{11}C]-(+)-4-propyl-3,4,4a,5,6,10b-hexahydro-2H-naphtho[1,2-b][1,4]oxazin-9-ol as a potential radiotracer for in vivo imaging of the dopamine D2 high-affinity state with positron emission tomography. *J Med Chem.* 2005;48:4153–4160.

2. Willeit M, Ginovart N, Kapur S, et al. High-affinity states of human brain dopamine D2/3 receptors imaged by the agonist [^{11}C]-(+)-PHNO. *Biol Psychiatry.* 2006;59:389–394.
3. Narendran R, Slifstein M, Guillin O, et al. Dopamine (D2/3) receptor agonist positron emission tomography radiotracer [^{11}C]-(+)-PHNO is a D3 receptor preferring agonist in vivo. *Synapse.* 2006;60:485–495.
4. Freedman SB, Patel S, Marwood R, et al. Expression and pharmacological characterization of the human D3 dopamine receptor. *J Pharmacol Exp Ther.* 1994;268:417–426.
5. Gallezot J-D, Beaver JD, Gunn RN, et al. Affinity and selectivity of [^{11}C]-(+)-PHNO for the D3 and D2 receptors in the rhesus monkey brain in vivo. *Synapse.* 2012;66:489–500.
6. Tziortzi AC, Searle GE, Tzimopoulou S, et al. Imaging dopamine receptors in humans with [^{11}C]-(+)-PHNO: dissection of D3 signal and anatomy. *Neuroimage.* 2011;54:264–277.
7. Rabiner EA, Laruelle M. Imaging the D3 receptor in humans in vivo using [^{11}C](+)-PHNO positron emission tomography (PET). *Int J Neuropsychopharmacol.* 2010;13:289–290.
8. Ginovart N, Willeit M, Rusjan P, et al. Positron emission tomography quantification of [^{11}C]-(+)-PHNO binding in the human brain. *J Cereb Blood Flow Metab.* 2007;27:857–871.
9. Innis RB, Cunningham VJ, Delforge J, et al. Consensus nomenclature for in vivo imaging of reversibly binding radioligands. *J Cereb Blood Flow Metab.* 2007;27:1533–1539.
10. Girgis RR, Xu X, Miyake N, et al. In vivo binding of antipsychotics to D_3 and D_2 receptors: a PET study in baboons with [^{11}C]-(+)-PHNO. *Neuropsychopharmacology.* 2011;36:887–895.
11. American Psychiatric Association. *Diagnostic and Statistical Manual of Mental Disorders* (DSM–IV), 4th ed. Washington, D.C.: American Psychiatric Association; 1994.
12. Ichise M, Toyama H, Innis RB, Carson RE. Strategies to improve neuroreceptor parameter estimation by linear regression analysis. *J Cereb Blood Flow Metab.* 2002;22:1271–1281.
13. Lammertsma AA, Hume SP. Simplified reference tissue model for PET receptor studies. *Neuroimage.* 1996;4:153–158.
14. Wu Y, Carson RE. Noise reduction in the simplified reference tissue model for neuroreceptor functional imaging. *J Cereb Blood Flow Metab.* 2002;22:1440–1452.
15. Willeit M, Ginovart N, Graff A, et al. First human evidence of d-amphetamine induced displacement of a D2/3 agonist radioligand: a [^{11}C]-(+)-PHNO positron emission tomography study. *Neuropsychopharmacology.* 2008;33:279–289.
16. Shrout PE, Fleiss JL. Intraclass correlations: uses in assessing rater reliability. *Psychol Bull.* 1979;86:420–428.
17. Searle GE, Beaver JD, Tziortzi A, et al. Mathematical modelling of [^{11}C]-(+)-PHNO human competition studies. *Neuroimage.* 2013;68:119–132.
18. Lee DE, Gallezot J-D, Zheng M-Q, et al. Test-retest reproducibility of [^{11}C]-(+)-propyl-hexahydro-naphtho-oxazin positron emission tomography using the bolus plus constant infusion paradigm. *Mol Imaging.* 2013;12:77–82.
19. Logan J, Volkow ND, Fowler JS, et al. Effects of blood flow on [^{11}C]raclopride binding in the brain: model simulations and kinetic analysis of PET data. *J Cereb Blood Flow Metab.* 1994;14:995–1010.
20. Alakurtti K, Aalto S, Johansson JJ, et al. Reproducibility of striatal and thalamic dopamine D2 receptor binding using [^{11}C]raclopride with high-resolution positron emission tomography. *J Cereb Blood Flow Metab.* 2011;31:155–165.
21. Narendran R, Frankle WG, Mason NS, et al. Positron emission tomography imaging of $D_{2/3}$ agonist binding in healthy human subjects with the radiotracer [^{11}C]-N-propyl-norapomorphine: preliminary evaluation and reproducibility studies. *Synapse.* 2009;63:574–584.
22. Kodaka F, Ito H, Kimura Y, et al. Test-retest reproducibility of dopamine D2/3 receptor binding in human brain measured by PET with [^{11}C]MNPA and [^{11}C]raclopride. *Eur J Nucl Med Mol Imaging.* 2013;40:574–579.

The Journal of NUCLEAR MEDICINE

Parametric Imaging and Test–Retest Variability of ^{11}C-(+)-PHNO Binding to D_2/D_3 Dopamine Receptors in Humans on the High-Resolution Research Tomograph PET Scanner

Jean-Dominique Gallezot, Ming-Qiang Zheng, Keunpoong Lim, Shu-fei Lin, David Labaree, David Matuskey, Yiyun Huang, Yu-Shin Ding, Richard E. Carson and Robert T. Malison

J Nucl Med. 2014;55:960-966.
Published online: April 14, 2014.
Doi: 10.2967/jnumed.113.132928

The Journal of Nuclear Medicine is published monthly.
SNMMI | Society of Nuclear Medicine and Molecular Imaging
1850 Samuel Morse Drive, Reston, VA 20190.
(Print ISSN: 0161-5505, Online ISSN: 2159-662X)

SNMMI SOCIETY OF NUCLEAR MEDICINE AND MOLECULAR IMAGING